

p -shell nuclei in a $(0+2)\hbar\omega$ model space. I. Method

A. A. Wolters, A. G. M. van Hees, and P. W. M. Glaudemans

Department of Physics and Astronomy, University of Utrecht, P.O. Box 80.000, 3508 TA Utrecht, The Netherlands

(Received 24 July 1990)

An empirical effective interaction for the $A=4-16$ p -shell nuclei in the complete $(0+2)\hbar\omega$ model space is presented, which also reproduces the predominant $2\hbar\omega$ intruder states. The results are not spoiled by the mixing catastrophe. The inclusion of $2\hbar\omega$ states also leads to a new feature not encountered before in smaller model spaces, i.e., the appearance of radially excited states. The latter can be observed experimentally in certain cases.

I. INTRODUCTION

The first systematic shell-model study for p -shell nuclei was published in 1965.¹ It was very successful and is still used for the interpretation of experimental data. The interaction with configuration mixing included was determined in the smallest model space possible for the p -shell nuclei, the $0\hbar\omega$ model space. In this space only normal-parity states can be described. During the last 20 years new and fast developments in the available computer facilities took place. This was the reason that large-scale shell-model calculations became feasible. For p -shell nuclei this resulted in 1983 in a publication² in which a mass-independent interaction was presented in the $(0+1)\hbar\omega$ model space. With that description one could treat both normal- and non-normal-parity states.

Despite the successes of these earlier calculations a number of discrepancies between theory and experiment remained. In particular the existence of intruder states was an unsolved problem. These are low-lying states in the spectrum which cannot be reproduced in the small $0\hbar\omega$ model space. Hence, it is a natural continuation of earlier calculations to treat the p -shell nuclei in the $(0+2)\hbar\omega$ model space.

The p -shell nuclei are good candidates to investigate in shell-model calculations. The two main reasons are (i) no inert core has to be assumed, since these nuclei contain a relatively small number of particles, and (ii) the j values of the p -shell orbits as well as those of the neighboring shells are relatively small. This makes it easier to expand the model space to include the neighboring shells.

In this paper we describe the methods used to obtain the present empirical effective interaction and the electromagnetic operators as well as some general results of the calculations.

The choice of the model space and the expansion of the interaction in terms of Talmi integrals are given in Secs. II and III, respectively. The approach to obtain the parameter values is outlined in Secs. IV–VII. Some properties of the resulting interaction are discussed in Sec. VIII.

The general agreement with experiment for the predominant $0\hbar\omega$ states and the intruder states is shown in Secs. IX and X. The methods used to identify the so-called radially excited states is presented in Sec. XI. The main conclusions are summarized in Sec. XII.

More detailed results for the various p -shell nuclei separately are given in paper II, see Ref. 3.

II. THE MODEL SPACE

The Hamiltonian is assumed to be translational invariant. The number of basis states, for which we chose harmonic oscillator states, is in principle infinite. Hence, one has to restrict the configuration space in order to obtain a finite number. But then it is possible that spurious and nonspurious states will mix, even for a translational invariant interaction. However, it has been shown that this problem of mixing does not occur in a complete $N\hbar\omega$ model space, with $N=0,1,2,\dots$. A complete $N\hbar\omega$ model space contains only basis states with an excitation of $N\hbar\omega$ above the Fermi level. In such a limited, but complete, space the Hamiltonian still commutes with the center-of-mass Hamiltonian, and therefore we can use the procedure for the exact elimination of the spurious states, described by van Hees *et al.*²

The calculations in this paper concern $0p$ -shell nuclei, i.e., nuclei with a mass $A=4-16$. The simplest model space for these nuclei is the $0\hbar\omega$ model space. In this space the s shell is completely filled and only the p shell is active. It is clear that in such a model space only states with $\pi=(-1)^A$, i.e., normal-parity states, can be calculated.

A next step is the inclusion² of particles in the sd shell or holes in the s shell. Allowing a single particle to move from the s shell into the p shell, or from the p shell into the sd shell makes it possible to describe the non-normal-parity states too. This gives us the $1\hbar\omega$ model space.

The next expansion of the model space is the $2\hbar\omega$ model space. This space contains all configurations where either two particles make a jump of $1\hbar\omega$ between two

neighboring major shells, i.e., from the s shell into the p shell and/or from the p shell into the sd shell, or a single particle makes a $2\hbar\omega$ jump, i.e., from the s shell into the sd shell or from the p shell into the fp shell. It should be remarked that in the $2\hbar\omega$ model space only states with normal parity can be calculated.

III. THE INTERACTION

For a translational invariant, isospin conserving two-body interaction V , which depends only on intrinsic coordinates, one obtains the following expression for the matrix elements between normalized and antisymmetrized two-particle states^{2,4}

$$\begin{aligned} \langle \rho_a \rho_b | V | \rho_c \rho_d \rangle_{JT} = & \frac{1}{2\sqrt{(1+\delta_{ab})(1+\delta_{cd})}} \\ & \times \sum_{\Lambda \Lambda' S} \begin{pmatrix} l_a & \frac{1}{2} & j_a \\ l_b & \frac{1}{2} & j_b \\ \Lambda & S & J \end{pmatrix} \begin{pmatrix} l_c & \frac{1}{2} & j_c \\ l_d & \frac{1}{2} & j_d \\ \Lambda' & S & J \end{pmatrix} \\ & \times \sum_{nl'n'l'} [(1-(-1)^{l+S+T})(1-(-1)^{l'+S+T}) \langle nlNL | n_a l_a n_b l_b \rangle_{\Lambda} \langle n'l'NL | n_c l_c n_d l_d \rangle_{\Lambda'}] \\ & \times \sum_j \begin{pmatrix} l & S & j \\ L & 0 & L \\ \Lambda & S & J \end{pmatrix} \begin{pmatrix} l' & S & j \\ L & 0 & L \\ \Lambda' & S & J \end{pmatrix} \langle n(lS)jT | V | n'(l'S)jT \rangle. \end{aligned} \quad (1)$$

The matrix elements $\langle n(lS)jT | V | n'(l'S)jT \rangle$ are referred to as relative matrix elements.

The next step consists of the assumption that the effective interaction V_{eff} can be decomposed in the following way

$$V_{\text{eff}} = \sum_{\nu T} V_{\nu T}(r) \Omega_{\nu} P_T, \quad (2)$$

where $V_{\nu T}$ is a radial potential and P_T is an isospin projection operator. The different operators Ω_{ν} , with ν labeling the central ($S=0, S=1$), tensor or spin-orbit parts, are defined with the Pauli spin operator σ as follows. The central spin projection operator on states with $S=0$ is

$$\Omega_{\text{central}, S=0} = \frac{1}{4}(1 - \sigma^{(1)} \cdot \sigma^{(2)}); \quad (3)$$

the central spin projection operator on states with $S=1$ is

$$\Omega_{\text{central}, S=1} = \frac{1}{4}(3 + \sigma^{(1)} \cdot \sigma^{(2)}); \quad (4)$$

the tensor operator is

$$\Omega_{\text{tensor}} = 3(\sigma^{(1)} \cdot \hat{r})(\sigma^{(2)} \cdot \hat{r}) - \sigma^{(1)} \cdot \sigma^{(2)}; \quad (5)$$

the spin-orbit operator is

$$\Omega_{LS} = \frac{1}{2} \ell \cdot (\sigma^{(1)} + \sigma^{(2)}), \quad (6)$$

where ℓ the relative two-particle orbital angular momentum.

With these expressions one can rewrite the relative matrix elements in (1) (see Lawson⁴):

$$\langle n(lS)jT | V_{S'T'}(r) \Omega_{\text{central}, S'} P_{T'} | n'(l'S)jT \rangle = \delta_{ll'} \delta_{SS'} \delta_{TT'} \langle nl | V_{S'T'}(r) | n'l' \rangle, \quad (7)$$

$$\begin{aligned} \langle n(lS)jT | V_{\text{tensor}T'}(r) \Omega_{\text{tensor}} P_{T'} | n'(l'S)jT \rangle = & (-1)^{j+1} 2\sqrt{6(2l+1)(2l'+1)} \\ & \times \langle 10l'0 | 20 \rangle \begin{Bmatrix} l & l' & 2 \\ 1 & 1 & j \end{Bmatrix} \delta_{S1} \delta_{TT'} \langle nl | V_{\text{tensor}, T'}(r) | n'l' \rangle, \end{aligned} \quad (8)$$

and

$$\langle n(lS)jT | V_{LS, T'}(r) \Omega_{LS} P_{T'} | n'(l'S)jT \rangle = \frac{1}{2}[j(j+1) - l(l+1) - S(S+1)] \delta_{ll'} \delta_{TT'} \langle nl | V_{LS, T'}(r) | n'l' \rangle. \quad (9)$$

A way to evaluate the radial matrix elements of V_{eff} , $\langle nl | V_{\nu T} | n'l' \rangle$, has been given by Talmi,⁵ where these matrix elements are expressed in terms of Talmi integrals $I_p^{(\nu T)}$ according to the relation

$$\langle nl | V_{\nu T} | n'l' \rangle = \sum_{p=(l+l')/2}^{n+n'+(l+l')/2} B(nln'l'; p) I_p^{(\nu T)}. \quad (10)$$

The Talmi integrals $I_p^{(\nu T)}$ are defined⁵ as

$$I_p^{(\nu T)} = \frac{\sqrt{2}}{b\Gamma(p+\frac{3}{2})} \int_0^{\infty} \left(\frac{r}{b\sqrt{2}} \right)^{2p+2} e^{-r^2/2b^2} V_{\nu T}(r) dr, \quad (11)$$

and the expansion coefficients $B(nln'l'; p)$ are given⁶ by

$$B(nln'l';p) = \frac{1}{2}\Gamma(p + \frac{3}{2}) \sum_{k=k_{\min}}^{k_{\max}} a_{nlk} a_{n'l'k'} \quad (12)$$

with $k' = p - \lambda - k$ and $\lambda = (l + l')/2$. The summation boundaries in (12) are $k_{\min} = \max(0, p - \lambda - n')$ and $k_{\max} = \min(n, p - \lambda)$. The factors a_{nlk} are the expansion coefficients of the associated Laguerre polynomial $L_n^{(l+1/2)}(x)$, given by

$$a_{nlk} = \frac{(-1)^k}{k!} \binom{n+l+\frac{1}{2}}{n-k} \left[\frac{2n!}{\Gamma(n+l+\frac{3}{2})} \right]^{1/2}. \quad (13)$$

Herewith we have explained the procedure to evaluate the two-body matrix elements of an effective interaction V_{eff} which is parametrized in terms of Talmi integrals.

It can be shown⁷ that of the $p=0$ Talmi integrals only two $I_{p=0}$ Talmi integrals contribute in an actual calculation: $I_{p=0}^{(\text{central}, S=0, T=1)}$ and $I_{p=0}^{(\text{central}, S=1, T=0)}$. Furthermore, of the $p=1$ Talmi integrals $I_{p=1}^{(LS, T=0)}$ does not contribute to any matrix element. The total number of Talmi integrals that contributes in a $(0+1+\dots+N)\hbar\omega$ model space for p -shell nuclei grows only linearly with N , and is equal to $13+N \times 8$.

IV. THE FITTING PROCEDURE

Talmi integrals can be evaluated in a phenomenological approach, i.e., the integrals are determined from a fit to a large set of experimental data.

We have made two important improvements in the fitting procedure during the last few years. The first one consists of the inclusion of static moments in the experimental data used for the determination of the interaction parameters. A detailed discussion about the consequences of an inclusion of these moments can be found in van Hees *et al.*⁸

The second extension, based to some extent on the work of Chung,⁹ is the possibility to assign an error to each parameter in the fit, which gives an indication whether the parameter is well determined or not. For a full discussion we refer to Wolters.⁷ In this paper we will only summarize the method.

In the fitting procedure one uses a set of equations, which describe the theoretically calculated observables. The parameters in the Hamiltonian and in the electromagnetic operators will be determined by fitting the calculated values to the corresponding experimental values. This requires an iterative process. The aim is that the finally obtained parameters will reproduce the experimental values of all included observables as well as possible.

In mathematical form one wants to solve the following set of linear equations for the parameter vector \mathbf{x}

$$\sum_{\beta=1}^{n_{\text{par}}} A_{\alpha\beta} x_{\beta} = b_{\alpha}, \quad 1 \leq \alpha \leq n_{\text{exp}}, \quad (14)$$

where n_{par} denotes the number of parameters and n_{exp} the number of experimental data. The symbol $A_{\alpha\beta}$ denotes the coefficient matrix (describing the Hamiltonian or electromagnetic operators), b_{α} are the experimental

values of the observables (e.g., level energies, static moments) and x_{β} the components of the parameter vector \mathbf{x} (in our case consisting of Talmi integrals, g factors and effective charges).

The function Q^2 one needs in the least-squares fit to solve (14) is given by

$$Q^2 = \sum_{\alpha} \left[\sum_{\beta} A_{\alpha\beta} x_{\beta} - b_{\alpha} \right]^2, \quad (15)$$

where the value of \mathbf{x} , which minimizes Q^2 , has to be determined. Weight factors for the experimental data are included in the matrix A and b .

One can then define two types of errors for each parameter x_i , the delta error δx_i and the epsilon error ϵx_i . For the delta error δx_i the value Q^2 remains smaller than $(1+\Delta)Q_{\min}^2$ if just this *one* parameter x_i is chosen in the interval $[x_i - \delta x_i, x_i + \delta x_i]$ around its optimum value x_i . All other parameters x_j with $j \neq i$ are kept fixed at their optimized values. The epsilon error ϵx_i of the parameter x_i is generally much larger than its delta error. It determines the range in which x_i may vary under the condition that *all* other parameters x_j with $j \neq i$ are optimized again.

The errors are defined such that, with the parameter values $x_i \pm \delta x_i$ or $x_i \pm \epsilon x_i$, the value of Q^2 will not increase more than a fraction Δ of the minimum value for Q^2 , denoted by Q_{\min}^2 . The δ and ϵ error thus gives an indication whether or not a certain parameter has a large effect on the results (δ error) and if it is strongly correlated with other parameters (ϵ error). Since Q^2 depends nonlinearly on the parameters, one should take a rather small value for Δ . In this calculation we take the value $\Delta = 0.05$ and thus Q_{\min}^2 may increase by 5%.

V. EXPERIMENTAL DATA

We start the discussion of experimental data to be included in the fitting procedure with the level energies. A separation will be made between levels which can be described in a $0\hbar\omega$ model space and those which cannot. We will call the latter intruder states.

The following criteria have been used to select the experimental data.

(i) All states should have a well assigned normal parity [$\pi = (-1)^A$]. This is evident, because only these states can be described in the $(0+2)\hbar\omega$ model space.

(ii) All included levels should have well-assigned spin and isospin quantum numbers.

(iii) Level energies are taken from $N \geq Z$ nuclei only. In general for these nuclei more experimental data are available than for the proton rich nuclei.

(iv) For the predominantly $0\hbar\omega$ levels, at most the lowest two states with given J^{π}, T are selected for each nucleus. The third or higher levels are in most nuclei experimentally uncertain, because of problems in spin, isospin and/or parity assignment. This criterium also holds for the intruder states. Exceptions are the third 1^+ state in ^{14}N , because it is the lowest-lying intruder state in this nucleus, and the third $\frac{3}{2}^-$ state in ^{15}N , which is also a well-known intruder state. Both states are included in the fit.

For the $A \leq 12$ nuclei only four intruder states are selected for the fit: the 0_2^+ states in ^4He , ^{10}Be , and ^{12}C and the 2_1^+ state in ^{12}Be . Other candidates for intruder states in these nuclei are not available; experimental spectra for these nuclei are incomplete or it is unclear to which calculated level an experimental state should be assigned. Most of the intruder states with a spin higher than the maximum value that can be obtained in the $0\hbar\omega$ model space are included. These states have been observed mainly in nuclei at the upper end of the p shell.

In total 109 states in the nuclei with $A = 4-16$ have been selected of which 36 are classified as intruder states. Furthermore, we included in the fit 18 experimentally known magnetic dipole moments and 12 electric quadrupole moments of the nuclei with $A = 4-16$. All experimental data have been taken from Ajzenberg.¹⁰⁻¹³ Exceptions are the data of ^4He , which have been taken from Fiarman *et al.*,¹⁴ and the quadrupole moment of ^7Li , where a recent and more accurate value from Weller *et al.*¹⁵ has been taken. The values of the binding energies for the ground states have been obtained from Wapstra *et al.*¹⁶

VI. COULOMB ENERGY

The interaction presented in Sec. III does not take into account the charge-dependent part of the interaction, i.e., the Coulomb energy. Therefore we have removed the charge-dependent contribution E_C from the experimental energies. The value of E_C is determined from a least-squares fit to experimental data. In the determination of E_C the following assumptions are made.

(i) E_C depends only on Z .

(ii) The difference between the contribution to E_C for different Z values is determined by the differences in the experimental energies of all known analog states in a corresponding isobaric multiplet.

In Table I the resulting empirical values for E_C are presented. To judge the correctness of these values, we performed a calculation in the $(0+1)\hbar\omega$ model space in the proton-neutron formalism. The advantage of using the proton-neutron formalism is the fact that the Coulomb interaction can be easily taken into account in the Hamiltonian. The interaction in this calculation was parametrized by $\hbar\omega$, 21 Talmi integrals, 6 parameters (effective nucleon g factors and charges) for the included static moments, and a strength parameter for the Coulomb energy. The relative matrix elements of the Coulomb interaction between two particles are those of the $1/r$ potential. All parameters have been determined in a fit of calculated energies and moments to 146 corresponding experimental energies and 39 static moments.

After reaching convergence of the fit, we calculated the Coulomb energy for each level. This energy is not necessarily the same for all levels with equal Z . Therefore this calculation yields a minimum and a maximum value of E_C for levels of each Z included in the fit. The latter E_C values are also presented in Table I. The correspondence between the empirical values and the calculated values in Table I is rather good. We conclude that the empirical E_C values are sufficiently accurate to estimate the influence of the Coulomb energy on the total binding energy.

VII. THE ITERATION PROCESS

The interaction is parametrized in 29 Talmi integrals and $\hbar\omega$. The inclusion of magnetic dipole and electric quadrupole moments leads to six extra parameters: four effective g factors and two effective charges. To determine the values of the interaction parameters we first constructed the Hamiltonian matrices of all states included in the fit. Furthermore, the matrices of the $\mathcal{M}1$ and/or $\mathcal{E}2$ operators, for those states of which the moments are included in the fit, were created. This was possible by using one and the same program: RITSSCHIL.¹⁷ With a set of numbers that occupy about 2 Gbyte the iteration process to determine the parameters could be started. One step in this process takes about 50 min CPU time on a vector computer as the Cyber 205 (2 pipes). The wall-clock time for one iteration step is about 1.5 h.

If one tries to determine all parameters at once, the fitting procedure does not converge. The strategy finally used consists of several stages, which were carried out one after the other. The parameters derived from one stage were used as starting parameters in the next stage. Each stage consists of roughly five iterations steps. For the detailed description of the iteration process we refer to Wolters.⁷

VIII. THE RESULTING INTERACTION

For the resulting interaction one obtains the root-mean-square deviations shown in Table II. These are the deviations between the experimental and calculated level energies and moments, which were included in the fitting procedure. For the energies we give the total rms deviation of all states in the first row of Table II and also the separated rms deviation for the states, which can be described in the $0\hbar\omega$ model space, and the one for the intruder states in the second and third row, respectively. For the static moments we give the rms deviation $\Delta\mu_{\text{rms}}$ for the magnetic dipole moments and ΔQ_{rms} for the quadrupole moments.

TABLE I. The values of the Coulomb energy E_C (MeV) for each Z . For an explanation of the different values, see text.

Z	^2He	^3Li	^4Be	^5B	^6C	^7N	^8O
Empirical E_C	0.76	1.46	3.12	5.02	7.72	10.56	14.06
Calculated E_C (min)	0.55	1.70	3.14	5.16	7.56	10.40	13.77
Calculated E_C (max)	0.68	1.70	3.33	5.25	7.77	10.65	14.10

TABLE II. rms deviations.

ΔE_{rms} total	0.56 MeV
ΔE_{rms} $0\hbar\omega$ levels	0.51 MeV
ΔE_{rms} intruder states	0.65 MeV
$\Delta\mu_{\text{rms}}$	$0.047\mu_N$
ΔQ_{rms}	0.23 efm^2

In Table III the parameters for the Hamiltonian are presented. The value of each parameter together with the δ and ϵ errors (see Sec. IV), which resulted from the fit, is given in this table as well.

Table IV contains the values of the parameters for the $\mathcal{M}1$ and $\mathcal{E}2$ operators with δ and ϵ errors. These parameters form the six extra parameters in the fitting procedure as a result of the inclusion of the static moments. The matrix elements of an $\mathcal{E}L$ operator are proportional to b^L , where b is the harmonic oscillator size parameter. Therefore one can extract from the fit to quadrupole moments only empirical values for the products b^2e_p and b^2e_n , and not the effective proton and neutron charge, e_p and e_n . The matrix elements of the $\mathcal{M}1$ operator are independent of the size parameter b , so effective g factors follow directly from the fit to the magnetic dipole moments. The consequences of this will be discussed in paper II.

TABLE III. Parameters ($\hbar\omega$ and Talmi integrals) of the Hamiltonian with errors (MeV).

Parameter	Value	δ error	ϵ error
$\hbar\omega$	+9.782	0.010	0.875
Central $S=0, T=0, p=1$	-1.756	0.034	2.058
$p=2$	+1.464	0.107	2.450
$p=3$	-0.678	0.150	4.350
Central $S=0, T=1, p=0$	-6.837	0.009	1.342
$p=1$	-2.749	0.028	1.192
$p=2$	-1.347	0.016	1.223
$p=3$	-0.144	0.068	1.685
$p=4$	+0.437	0.192	2.636
Central $S=1, T=0, p=0$	-8.592	0.009	1.595
$p=1$	-3.893	0.031	1.212
$p=2$	-2.623	0.016	1.130
$p=3$	-1.633	0.082	1.924
$p=4$	-0.432	0.217	4.098
Central $S=1, T=1, p=1$	+1.748	0.004	0.342
$p=2$	-0.193	0.017	0.231
$p=3$	-1.899	0.021	0.473
Spin-orbit $T=0, p=2$	+0.270	0.034	0.355
$p=3$	+0.248	0.094	0.762
$p=4$	-0.472	0.205	2.017
Spin-orbit $T=1, p=1$	-1.251	0.015	0.267
$p=2$	-0.391	0.048	0.293
$p=3$	-0.203	0.034	0.305
Tensor $T=0, p=1$	+1.581	0.113	0.887
$p=2$	+1.223	0.096	0.798
$p=3$	+0.501	0.173	1.358
$p=4$	-0.971	0.437	3.077
Tensor $T=1, p=1$	-0.117	0.061	0.829
$p=2$	+1.190	0.040	0.752
$p=3$	-0.327	0.068	0.577

TABLE IV. Parameters of the $\mathcal{M}1$ and $\mathcal{E}2$ operator with errors.

Parameter	Value	δ error	ϵ error
g_l^p	+1.183	0.053	0.069
g_l^n	-0.137	0.058	0.071
g_s^p	+5.906	0.113	0.170
g_s^n	-4.175	0.133	0.186
$b^2e_p(\text{efm}^2)$	+3.625	0.218	0.717
$b^2e_n(\text{efm}^2)$	+0.178	0.197	0.647

It is interesting to investigate whether conclusions about the nature of the effective interaction can be drawn from the present empirical set of Talmi integrals. The definition of Talmi integrals, (11), implies that the absolute values of the Talmi integrals for a short-range interaction decrease rather strongly for increasing p . Furthermore, negative values for all Talmi integrals I_p means that the corresponding potential is attractive, while positive values indicate repulsion. Finally, a change in sign of the value of the Talmi integrals for increasing p indicates a repulsive potential for short distances that becomes attractive at larger distances, or vice versa.

It follows from the errors of all parameters presented in Table III that in particular the $p \geq 3$ and the central $S=0, T=0$ integrals are poorly determined. The largest δ errors ($\gtrsim 0.2$) belong to the $p=4$ Talmi integrals. Thus these parameters occur with the smallest coefficients in the equations used in the least-squares fit. It means that effects of possible long-range parts of the interaction are not clearly visible.

Another general remark concerns the differences in the values of the δ and ϵ errors of each parameter. A relatively large ϵ errors means that the parameter is strongly correlated with other parameters. An example is the central $S=1, T=0, p=0$ Talmi integral. In general this can be said of all central Talmi integrals. Each of them is rather well determined when all other parameters are kept fixed, but their mutual correlations make them less accurately determined.

The $S=0, T=1$ and $S=1, T=0$ channels clearly show an attractive character. For the others channels no conclusions are drawn, since the numerical values of the Talmi integrals are not well enough determined.

IX. PREDOMINANTLY $0\hbar\omega$ STATES

It follows from Table II that the total rms deviation for all states included in the fit is given by $\Delta E_{\text{rms}} = 0.56 \text{ MeV}$. The ΔE_{rms} can be separated into a deviation for the levels with mainly a $0\hbar\omega$ character and one for the intruder states. In this section we will restrict ourselves to the levels of the first kind. The rms deviation for these levels is equal to 0.51 MeV. It is interesting to compare this value with that of other calculations. Therefore we present in Table V the rms deviations for $0\hbar\omega$ levels for several interactions obtained earlier for p shell nuclei. All these interactions are mass independent and have been determined from approximately 75 levels in the complete p shell, i.e., $A=4-16$, except for the $(8-16)\text{POT}$ of Cohen

and Kurath,¹ who included only 35 levels in the nuclei $A=8-16$. The rms deviation for the (8-16)POT, presented in Table V, is obtained by calculating the binding energies of the present, much larger set of 75 levels.

From Table V one sees a significant improvement for the present calculation concerning the overall rms deviation compared to the other calculations. Furthermore it is interesting to observe that the rms deviation of a previous calculation, taking into account only the 13 lowest-order Talmi integrals in a mixed $(0+2)\hbar\omega$ model space,¹⁸ is considerably reduced by the inclusion of all 29 Talmi integrals. These 16 additional Talmi integrals contribute to matrix elements of the Hamiltonian between two $2\hbar\omega$ states or between a $0\hbar\omega$ and a $2\hbar\omega$ state, but not to matrix elements between two $0\hbar\omega$ states.

It is interesting to refer here also to our recently obtained results in a $0\hbar\omega$ space in which three-body forces have been taken into account as well.^{19,20} The latter procedure considerably improves the description of $0\hbar\omega$ states. However, it cannot treat intruder states.

X. INTRUDER STATES

In the past one of the major problems, when increasing the model space from $0\hbar\omega$ to $(0+2)\hbar\omega$, was the far too strong repulsion resulting from the mixing of several $2\hbar\omega$ states with $0\hbar\omega$ states,^{21,22} the so-called "mixing catastrophe."²³ Some formal studies of this mixing concern the renormalization of realistic interactions in limited model spaces^{24,25} and not the construction of an empirical interaction.

In previous calculations on p -shell nuclei the values of the Talmi integrals were determined by a fit, where intruder states were excluded. In such calculations the low-lying $0\hbar\omega$ states are pushed down by the new $2\hbar\omega$ states. If one tries to reproduce the binding energies of these low-lying $0\hbar\omega$ states by a simple renormalization of the interaction, then the problem persists in a similar way. The $0\hbar\omega$ states will be calculated at the correct energy, the intruder states will be shifted to much higher energies and will be obtained far too high in the spectrum.

However, with the present interaction a solution is found by the inclusion of 36 intruder states in the fitting procedure to determine the values of the Talmi integrals. This approach gave a good overall fit to all levels included. The inclusion of the intruder states in the fitting procedure apparently modified the interaction such that, without configuration mixing between the $0\hbar\omega$ and $2\hbar\omega$ spaces, the lowest $0\hbar\omega$ state in a nucleus is calculated far

above the lowest $2\hbar\omega$ state. With the same interaction applied in the mixed $(0+2)\hbar\omega$ model space, the low-lying $0\hbar\omega$ states are pushed down due to mixing with mainly higher-lying $2\hbar\omega$ states and end up below the $2\hbar\omega$ states. So the mixing of $0\hbar\omega$ and $2\hbar\omega$ model spaces causes again a very large shift of energy levels. However, in contrast with previous calculations we obtain in the present approach that this mixing shifts the predominantly $0\hbar\omega$ states to roughly the correct position.

One should emphasize here that the present interaction cannot be used in the small $0\hbar\omega$ model space, since the shell-model picture would completely break down if, for a realistic interaction, the pure $2\hbar\omega$ states would indeed lie below the $0\hbar\omega$ states.

The resulting rms deviation $\Delta E_{\text{rms}}=0.65$ MeV for intruder states shows that it is possible to describe these states in an acceptable way using all 29 Talmi integrals. This is in contrast with a previous $(0+2)\hbar\omega$ calculation,¹⁸ in which only 13 of the 29 Talmi integrals were determined. With that interaction it was not possible to reproduce the intruder states, because of the mixing catastrophe. This demonstrates the necessity to parametrize the interaction with all 29 Talmi integrals, and not only with the 13 lowest-order integrals. Moreover, the inclusion of the intruder states as input for the fitting procedure is essential. Their omission would not lead to a strongly improved description of the predominantly $0\hbar\omega$ states, but the fitting procedure becomes even less stable than it already is in the present calculation.

In total 36 intruder states were included in the fitting procedure. Compared to the rms deviation of the predominantly $0\hbar\omega$ levels, $\Delta E_{\text{rms}}=0.51$ MeV, it follows that the binding energies of the intruder states are not calculated with the same accuracy, since their rms deviation is $\Delta E_{\text{rms}}=0.65$ MeV. However, the use of the $(0+2)\hbar\omega$ model space gives the first opportunity to describe them, and we expect a more accurate description in a space where $4\hbar\omega$ components are also taken into account, see Hayes *et al.*²⁶

XI. RADIAL EXCITATIONS

In this section an interesting effect will be discussed. During our calculations we noticed that in several of the calculated spectra some levels appear with a relatively low excitation energy, which cannot be identified with experimental states.

As an example we will take the spectrum of ${}^8\text{Be}$. In Fig. 1 we show the lowest four calculated 0^+ and 2^+ states together with the experimentally known states with

TABLE V. rms deviations for the same set of 73 predominantly $0\hbar\omega$ levels in $A=4-16$ nuclei for several interactions.

Hamiltonian parameters	Reference	Model space	rms deviation (meV)
2 single-particle energies + 11 two-body matrix elements	Cohen <i>et al.</i> ¹	$0\hbar\omega$	1.07
$\hbar\omega+21$ relative matrix elements	van Hees <i>et al.</i> ²	$(0+1)\hbar\omega$	0.75
$\hbar\omega+13$ Talmi integrals	Wolters <i>et al.</i> ¹⁸	$(0+2)\hbar\omega$	0.68
$\hbar\omega+29$ Talmi integrals	Present calculation	$(0+2)\hbar\omega$	0.51

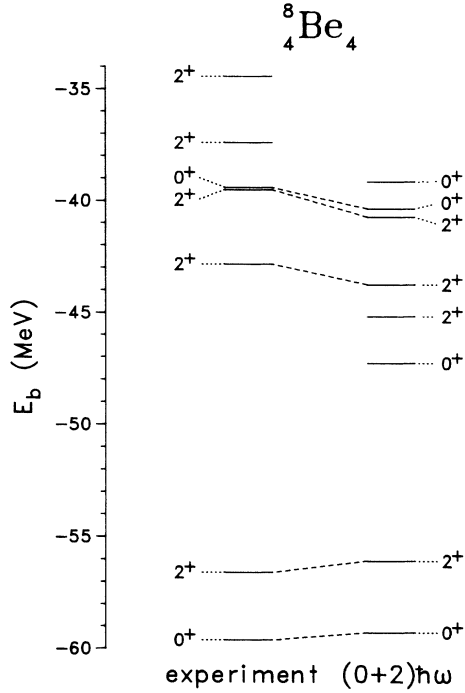


FIG. 1. Experimental and lowest four calculated 0^+ and 2^+ states in ${}^8\text{Be}$.

the same spins and parities. There is a very poor agreement with the excitation energy of the second experimental 0^+ state. However, at higher excitation energy there are two other theoretical candidates for this experimental state. With the assignments made in Fig. 1 the calculated second 2^+ state also has no experimental counterpart. The appearance of these additional levels is not a drawback of the present effective interaction, but an effect due to the discretization of continuum states, as will be discussed below.

The additional states can be classified as *radial excitations*. States belonging to this classification have always a companion at a lower binding energy with the same quantum numbers $J^\pi; T$. By the term radial excitation of the low-lying member we mean that the angular part of the wave function of the higher-lying member state is about the same as that of its low-lying companion. The radial part, however, has changed, because a particle has made a jump to a different major shell, e.g., $0p \rightarrow 1p$, so a change in the harmonic-oscillator radial quantum number n . Because such an excitation corresponds with an additional harmonic-oscillator kinetic energy of $1\hbar\omega$, i.e., $2 \times \frac{1}{2}\hbar\omega$, the high-lying state is expected at about $1\hbar\omega$ above the energy of its low-lying companion. However, effects of configuration mixing may change the energy of the radially excited state. We should emphasize here that the radially excited states are nonspurious. The spurious states with the center of mass in a $N=1, L=0$ state, that have the same structure as the radially excited states are removed from the low part of the spectrum according to the procedure explained in Ref. 2.

Let us consider again ${}^8\text{Be}$. This nucleus is particle unstable, since ${}^8\text{Be}$ decays in about 10^{-16} s into two α parti-

cles. This decay process leads to a continuum in the energy spectrum. One can consider the calculated low-lying states, which belong to the class of radial excitations, as a simulation of this continuum by a very limited number of discrete states. Because their spatial symmetry can be written as $[f]=[44]$, they can be identified as 2α clusters. It also implies that in a much larger model space, one expects to find a large number of such 0^+ states representing the continuum above the breakup threshold for ${}^8\text{Be}$, which lies 0.09 MeV below the ground state energy.

We suggest a possible way to identify the radial excitations by using the operator $r^2 = \sum_k^A r_k^2$, where A is the number of nucleons. This is the essential part of the isoscalar electric monopole operator $O(\mathcal{E}, L=0, M=0)$. It has vanishing matrix elements for transitions $0\hbar\omega \leftrightarrow 0\hbar\omega$ or $2\hbar\omega \leftrightarrow 2\hbar\omega$, but nonvanishing matrix elements between $0\hbar\omega$ and $2\hbar\omega$ states. It is also used to identify breathing modes.²⁷

We thus calculated the reduced matrix elements $\langle \Psi_f \| \sum_k^A r_k^2 \| \Psi_i \rangle$. The initial state Ψ_i and final state Ψ_f are wave functions with identical $J^\pi; T$, where Ψ_i represents the yrast state. If we take for Ψ_f all wave functions with the considered $J^\pi; T$ combination, except Ψ_i , we can also obtain the ratio R_f defined as

$$R_f = \frac{(\langle \Psi_f \| \sum_k^A r_k^2 \| \Psi_i \rangle)^2}{\sum_{f'} (\langle \Psi_{f'} \| \sum_k^A r_k^2 \| \Psi_i \rangle)^2} \quad \text{for } f, f' \neq i. \quad (16)$$

A small value for R_f means that Ψ_f cannot be considered as a radial excitation of Ψ_i , while a large value means the opposite. Therefore the operator r^2 might be useful for identifying the radial excitations. In Table VI we show

TABLE VI. Calculated total summed r^2 strength with and R_f values for several 0^+ excited states. See text for further explanation.

Nucleus	Total strength (b^4)	Ψ_f	$100 \times R_f$
${}^4\text{He}$	0.30	0_2^+	86.9
		0_3^+	1.0
		0_4^+	6.5
${}^8\text{Be}$	10.00	0_2^+	72.5
		0_3^+	1.5
		0_4^+	13.5
${}^{12}\text{C}$	11.73	0_2^+	46.0
		0_3^+	0.0
		0_4^+	0.0
${}^{14}\text{C}$	16.95	0_2^+	3.5
		0_3^+	17.8
		0_4^+	48.4
${}^{16}\text{O}$	19.60	0_2^+	19.3
		0_3^+	20.6
		0_4^+	30.4

the obtained ratios, defined in (16), as $100 \times R_f$ for the lowest excited 0^+ states in ${}^4\text{He}$, ${}^8\text{Be}$, ${}^{12}\text{C}$, ${}^{14}\text{C}$ and ${}^{16}\text{O}$. Besides, the total summed r^2 strength is presented. From this table it follows that in ${}^4\text{He}$, ${}^8\text{Be}$, and ${}^{12}\text{C}$ the radial excitation of the ground state is mainly concentrated in the 0_2^+ state, whereas in ${}^{14}\text{C}$ and ${}^{16}\text{O}$ the r^2 strength is much more fragmented. In ${}^{14}\text{C}$ the 0_2^+ state is not a radially excited state, since it can be reproduced already in the $0\hbar\omega$ model space. It should be noted that the total summed strengths in the current $(0+2)\hbar\omega$ calculation are smaller than the ones built on pure $0\hbar\omega$ states, for which sum rules are published.²⁷ This is a consequence of two effects. First, the $2\hbar\omega$ components in the ground state produce some r^2 strength for $4\hbar\omega$ states that are not in the model space. The second effect consists of the fact that the presence of $2\hbar\omega$ components in the wave functions leads in general to destructive interference.

Experimentally, some of these 0_2^+ states are observed, while others are not found. The reason for this is the threshold above which a nucleus becomes particle unstable. If the radially excited state lies below this threshold, it can be measured experimentally as a bound state in the spectrum. However, if it lies well above the threshold, it is not possible to observe this level experimentally, because it is part of the continuum, as a result of the fast decay of the nucleus. The third possibility is that one finds it close to the threshold, which means in practice that it is observed experimentally.

Consider again the 0_2^+ states given in Table VI, which are identified as radial excitations. The 0_2^+ states in ${}^4\text{He}$ and ${}^{12}\text{C}$ are obtained close to the threshold and therefore are also observed experimentally. The 0_2^+ state in ${}^8\text{Be}$ cannot be observed, because it is calculated far above the breakup threshold. In particular in ${}^8\text{Be}$ one should therefore expect a considerable amount of $\mathcal{E}0$ strength in the continuum at low energies. In this case it might be very difficult to detect this strength experimentally, however.

Because the operator r^2 is also involved in the calculation of $B(\mathcal{E}0)$ values, we present in Table VII the matrix elements $\langle \Psi_f || \sum_k^n r_k^2 || \Psi_i \rangle$, where n_p denotes the number of protons. We compare our calculated matrix elements with the experimentally known values.^{27,28} It follows that the theoretical values are about 30% too small, but that the relative numbers are very well reproduced.

Furthermore, it should be mentioned that states, which can be considered as a part of the discretization of the continuum, might have been also obtained in other calculations. However, note that these states cannot be classified as radially excited states. An example is the $\frac{1}{2}^+$ state at $E_x \approx 8.5$ MeV in ${}^5\text{He}$ ($\alpha+n$ in a relative $n=1, l=0$ orbit) for an interaction in the $(0+1)\hbar\omega$ model space.² For this very broad state one has observed $l=0$ spectroscopic strength in the proton-knockout reaction ${}^6\text{Li}(e, e'p)$ below $E_x = 16$ MeV in ${}^5\text{He}$.²⁹ Another exam-

TABLE VII. Calculated and experimental (Refs. 27 and 28) values for the matrix elements $\langle \Psi_f || \sum_k^n r_k^2 || \Psi_i \rangle$ (fm^2).

Nucleus	Ψ_f	Calculated	Experiment
${}^4\text{He}$	0_2^-	0.77	1.10 ± 0.16
${}^{12}\text{C}$	0_2^-	3.56	5.37 ± 0.22
${}^{16}\text{O}$	0_2^-	2.98	3.66 ± 0.55
	0_3^-	3.08	
	0_4^-	3.73	4.40 ± 0.44
	0_5^-	2.08	3.3 ± 0.7

ple is the first 1^- state in ${}^8\text{Be}$ ($\alpha+\alpha$ in a relative $n=2, l=1$ orbit), obtained with another interaction also in the $(0+1)\hbar\omega$ model space.²⁰

Summarizing, the following criteria have been used to identify radially excited states:

(i) The value of the ratio R_f defined in (16) should be ≥ 0.5 .

(ii) The energy should be roughly about $1\hbar\omega$ above the predominantly $0\hbar\omega$ yrast state with the same J^π and T .

A radially excited state might belong to the discretization of the continuum if its energy is well above the threshold for decay by particle emission and its symmetry corresponds with the symmetry of the open channel.

XII. CONCLUSIONS

The main conclusions from the present approach to correlate a large number of observables in $A=4-16$ nuclei with a mass-independent phenomenological interaction are given in the following points.

The average deviation between theoretical and experimental level energies is considerably smaller than in previous calculations.

Properties of many intruder states can be reproduced correctly.

Although the mixing between $0\hbar\omega$ and $2\hbar\omega$ states can be very strong, the mixing catastrophe can be avoided.

The expansion of the model space gives rise to the presence of radially excited states.

In a subsequent paper³ the spectra of many nuclei, the structure of the obtained wave functions, and the values of several observables will be presented. More additional information about the present results can be found in Ref. 7, which is available upon request.

This work was performed as part of the research program of the Stichting voor Fundamenteel Onderzoek der Materie (FOM) with financial support from the Nederlandse Organisatie voor Wetenschappelijk Onderzoek (NWO). The numerical calculations for this work were performed on a CDC-205 computer with financial support from the Stichting SURF through the Nationaal Fonds gebruik Supercomputers (NFS).

¹S. Cohen and D. Kurath, Nucl. Phys. **73**, 1 (1965).

²A. G. M. van Hees and P. W. M. Glaudemans, Z. Phys. A **314**, 343 (1983); **315**, 223 (1984).

³A. A. Wolters, A. G. M. van Hees, and P. W. M. Glaudemans, Phys. Rev. C **42**, 2062 (1990), the following paper.

⁴R. D. Lawson, *Theory of the Nuclear Shell Model* (Clarendon, Oxford, 1980).

⁵I. Talmi, Helv. Phys. Acta **25**, 185 (1952).

⁶T. A. Brody and M. Moshinsky, *Tables of Transformation Brackets* (Monografías del Instituto de Física, Mexico, 1960).

- ⁷A. A. Wolters, Ph.D. thesis, Utrecht University, 1989.
- ⁸A. G. M. van Hees, A. A. Wolters, and P. W. M. Glaudemans, Phys. Lett. B **196**, 19 (1987); Nucl. Phys. **A476**, 61 (1988).
- ⁹W. Chung, Ph.D. thesis, Michigan State University, 1976.
- ¹⁰F. Ajzenberg-Selove, Nucl. Phys. **A413**, 1 (1984).
- ¹¹F. Ajzenberg-Selove, Nucl. Phys. **A433**, 1 (1985).
- ¹²F. Ajzenberg-Selove, Nucl. Phys. **A449**, 1 (1986).
- ¹³F. Ajzenberg-Selove, Nucl. Phys. **A460**, 1 (1986).
- ¹⁴S. Fiarman and W. E. Meyerhof, Nucl. Phys. **A206**, 1 (1973).
- ¹⁵A. Weller, P. Egelhof, R. Čaplar, O. Karban, D. Krämer, K.-H. Möbius, Z. Moroz, K. Rusek, E. Steffens, G. Tungate, K. Blatt, Ilse Koenig, and D. Fick, Phys. Rev. Lett. **55**, 480 (1985).
- ¹⁶A. H. Wapstra and G. Audi, Nucl. Phys. **A322**, 1 (1985).
- ¹⁷D. Zwarts, Comput. Phys. Commun. **38**, 365 (1985).
- ¹⁸A. A. Wolters, A. G. M. van Hees, and P. W. M. Glaudemans, Europhys. Lett. **5**, 7 (1988).
- ¹⁹A. G. M. van Hees, J. G. L. Booten, and P. W. M. Glaudemans, Phys. Rev. Lett. **62**, 2245 (1989); **62**, 3099(E) (1989).
- ²⁰A. G. M. van Hees, J. G. L. Booten, and P. W. M. Glaudemans, Nucl. Phys. **A507**, 55c (1990).
- ²¹P. W. M. Glaudemans, in *Microscopic Approaches to Nuclear Structure Calculations*, edited by A. Covelto (Societa Italiana di Fysica, Bologna, 1986), p. 3.
- ²²D. J. Millener, D. I. Sober, H. Crannell, J. T. O'Brien, L. W. Fagg, S. Kowalski, C. F. Williamson, and L. Lapikás, Phys. Rev. C **39**, 14 (1989).
- ²³E. K. Warburton, private communications.
- ²⁴P. J. Ellis and L. Zamick, Ann. Phys. (N.Y.) **55**, 61 (1969).
- ²⁵P. J. Ellis, in *Windsurfing the Fermi Sea*, edited by T. T. S. Kuo and J. Speth (Elsevier, Amsterdam, 1987), Vol. II, p. 206.
- ²⁶A. C. Hayes, J. L. Friar, and D. Strottman, Phys. Rev. C **41**, 1727 (1990).
- ²⁷M. W. Kirson, Nucl. Phys. **A257**, 58 (1976).
- ²⁸H. Theissen, Springer Tracts Mod. Phys. **65**, 1 (1972).
- ²⁹J. B. J. M. Lanen, A. M. van den Berg, H. P. Blok, J. F. J. van den Brand, C. T. Christou, R. Endt, A. G. M. van Hees, E. Jans, G. J. Kramer, L. Lapikás, D. R. Lehman, W. C. Parke, E. N. M. Quint, G. van der Steenhoven, and P. K. A. de Witt Huberts, Phys. Rev. Lett. **62**, 2925 (1989).